ECO-EFFICIENT MELTING OF GLASS FRITS BY CONCENTRATED SOLAR ENERGY

M. Romero[a*], J. I. Robla[b], I. Padilla[b], J. García-Hierro[b], A. López-Delgado[b]

[a]*Eduardo Torroja Institute for Construction Sciences, IETcc-CSIC. C/ Serrano Galvache 4 – 28033 Madrid, Spain*

[b] *National Centre for Metallurgical Research, CENIM-CSIC. Av. Gregorio del Amo 8 – 28040 Madrid, Spain*

Abstract

This research aims to study the feasibility of applying real concentrated solar radiation to achieve the energy needed for melting glass frits. For this purpose, five glass compositions corresponding to different types of commercial frits were prepared. For comparison, the batches were melted by both in a solar furnace using concentrated solar energy (CSE) and in an electric furnace. The final frits were characterised by means of X-ray Fluorescence, X-ray Diffraction, Differential Thermal Analysis, Field Emission Scanning Electron Microscopy and Fourier Transformed Infrared Spectrometry. Results show that the frits prepared by CSE present short-range order, thermal behaviour and microstructure analogous to frits prepared in electric furnace. Moreover, the use of CSE for manufacturing glass frits reduces the melting time in about 80%, which leads to both lower corrosion of crucible wall and lower boron volatilization.

Keywords: glass frits, concentrated solar energy, microstructure, thermal behavior

* Corresponding author, Tel.: +34 91 302 04 40; Fax: + 34 91 302 07 00.

e-mail address: mromero@ietcc.csic.es

1. Introduction

Glass frits are glassy materials prepared by melting a mixture of raw materials at high temperature. Frits are the main component of nearly all ceramic glazes and they are also present in many compositions of different materials where a glassy phase is needed as binder. Currently, on the market there are many varieties of frits, with different fusibility, brightness, opacity and shading characteristics.

Nowadays, the production of frits is conducted in continuous melting furnaces and common temperatures in furnaces ranging between 1350º and 1550ºC. Once the raw materials batch is melted, it is cooled on water at high cooling rate; thus, the melt solidifies as small pieces of glass. This melting process implies a significant energy consumption and low efficiency and productivity of the process.

Frit manufacture is a highly intensive energy process, requiring high temperature usually provided by burning fossil fuels. The highest energy consumption of the process occurs inside the melting oven; in general, the energy necessary for melting accounts for over 75% of all energy consumed in the frit manufacturing process. The theoretical energy required to convert the raw materials mixture into glass is around 2.7 GJ/t (Trier, 1987), (Scalet et al., 2013). This theoretical value takes only into account the chemical heat of reaction and the enthalpy changes associated with heating up the batch from room temperature to the melting temperature. However, from a practical point of view it is required to overcome heat losses linked with upholding the glass melt temperature. The real energy consumption for modern industrial glass melting can vary from 3.5 to 40 GJ/t depending on furnace design and scale (Scalet et al., 2013). Thus, it is of great importance to search new sustainable melting techniques for diminishing the use of non-renewable energy.

In that sense, solar energy is nearly limitless and it can be concentrated to promptly supply high temperature. Important research work has been carried out aimed to use concentrated solar energy (CSE) in different industrial processes, such as the production of lime from limestone (Meier et al., 2005), alumina from boehmite (Padilla et al., 2014) and anhydrite from gypsum (López-Delgado et al., 2014). CSE has also been applied for sintering of alumina (Román et al., 2008) and cordietie-based ceramics (Costa Oliveira et al., 2005) and to metallurgical processes such melting of aluminium from aluminium scrap (Funken et al., 2001), production of titanium foams (García et al., 2016) recovery of zinc from zinc containing materials, (Tzouganatos et al., 2013) tempering of steels (Vázquez et al., 1991), production of titanium nitride (Sierra and Vázquez, 2005) and stainless steel (de Damborenea et al., 1994) coatings, welding of steels and titanium alloys (Romero et al., 2013) and thermal shock tests on intermetallic materials (Morris et al., 2015). However, no research has been previously conducted aiming to use CSE for producing glasses or glassy materials such as glass frits or glass enamels. Recently, the feasibility of using high flux solar simulator to provide a sustainable source of process heat for glass production was investigated (Ahmad et al., 2014). Initial experiments involved melting a ternary common soda–lime–silica (SLS) glass batch, which demonstrated that rapid and full conversion of the crystalline raw materials into an X-ray amorphous vitreous state was possible. The possibility of apply CSE to create a light-beam technology for obtaining art objects with a glass enamel coating has been also explored (Otmakhov, 2015). However, it is necessary to point out that the last two works did not use real CSE to achieve the necessary process energy. Instead, a high flux solar simulator consisting of xenon arc lamps, whose radiation spectrum is close to the solar spectrum, was used as sources of heat.

The aim of this research is to study the feasibility of applying real concentrated solar radiation to achieve the energy needed for performing, in only one step, the preparation of glass frits of different typology, from the raw materials. Thus the process includes decarbonation, melting and homogenization of molten fluids. To our knowledge, it is the first time that such a study has been undertaken.

2. Experimental

2.1 Materials and method

Five glass compositions were formulated with the aim of preparing different types of commercial frits, namely, crystalline (C); white of zirconium (WZr); middle fusibility (MF); fluxing (F) and matte of titanium (MTi). The compositions of the starting frits are shown in Table 1. Moreover, for evaluating the efficacy of concentrated solar radiation (CSE) for melting and homogenisation of molten fluids with different viscosity, the theoretical melting temperature (T_m) for the studied compositions, was determined according to the Fluegel´s Model for predicting the complete viscosity curve of glasses, by using polynomial functions for estimating the temperature-viscosity behaviour of silicate glasses from their chemical composition (Fluegel, 2007). The melting temperature is considered as that at which the viscosity of molten glass is 10^2 dPa s. Calculated T_m values are also reported in Table 1.

The raw materials used to prepare the glasses were: silica sand with low contents of iron oxide and reagent grade oxide such as Al_2O_3, B_2O_3, ZnO, PbO and ZrO_2. To complete the glasses composition alkali and alkaline earth elements were introduced as reagent grade carbonates. Mixtures were homogenised in a planetary ball mill (TURBULA) for 15 min. In order to compare the properties of frits obtained by melting in a solar furnace using concentrated thermal radiation, the same experiments were carried out using a

conventional electric furnace. In both cases, experiments were performed using tabular alumina crucibles and 35 g of the mixture of raw materials. After the required time to complete the decarbonation, fusion and homogenization stages, the glass frits were obtained by pouring the low-viscosity melts into cool water.

Table 1. Starting chemical composition (wt. %) of the investigated glasses.

	C	WZr	MF	F	MTi
SiO_2	50	50	40	50	40
B_2O_3	15	15	10	20	20
Al_2O_3	4	4	2	---	2
Na_2O	3	---	4	10	2
K_2O	---	---	---	10	---
Li_2O	3	7	3	---	2
CaO	8	4	6	10	2
BaO	2	2	2	---	25
ZnO	5	8	3	---	7
PbO	10	---	30	---	---
ZrO_2	---	10	---	---	---
T_m (ºC)	993	1079	822	880	885

For experiments carried out by CSE, a Medium Size Solar Furnace (MSSF) of CNRS-PROMESS Solar facilities (Font Romeu-Odeillo, France) was used. The solar furnace of 0.9 kW equipped with a vertical axis parabolic reflector of 1.5 m diameter produces a focal spot, ca. 15 mm in diameter, with a very high power density (1000 W/m^2). To control the incident solar radiation a shutter is positioned between the parabolic concentrator (placed in a 6^{th} floor level) and the heliostat (placed on first floor level). Temperature was measured by a type K thermocouple, which was positioned at half height of crucible. This vertical configuration is the only one that allows the heat treatment of powdered materials. Figure 1 shows the crucible receiving the solar radiation concentrated by the parabolic reflector.

Fig. 1. Parabolic solar concentrator.

The temperature-time register followed for the experiment to produce glass frits in both the electric furnace and the solar furnace are shown in Fig. 2. In the case of the experiments with CSE, the temperature was registered by a thermocouple placed outside in the crucible bottom.

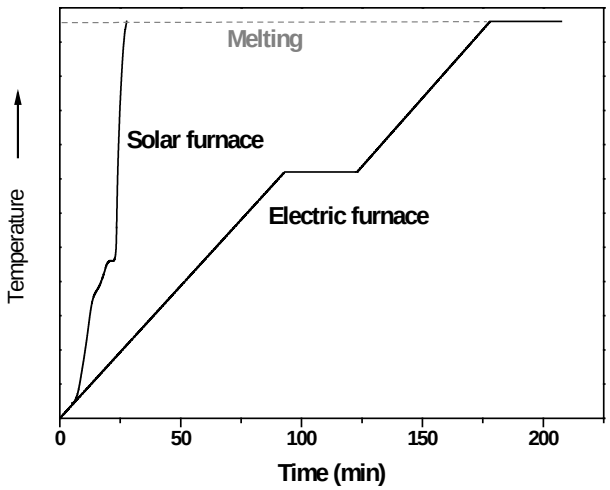

Fig. 2. Temperature-Time schedule used for raw materials melting in both solar and electric furnace.

2.2. Characterization techniques

Glass frits were characterised for determining if the type of energy, power density and thermal schedule used in their preparation lead to materials with the same physical-

chemical characteristics. The chemical analysis of frits was determined by X-ray fluorescence (XRF) using a Bruker S8 Tiger spectrometer. The analysis was performed on pressed pellets of powder glass samples (< 63 μm). B_2O_3 and Li_2O were determined by inductively coupled plasma optical emission spectrometry (ICP-OES) in a Varian 725-ES equipment. The evaluation of the amorphous nature of the frits after melting was performed by X-ray diffraction (XRD) using Bruker D8 Advance equipment with Ni-filtered Cu Kα radiation operating at 30 mA and 40 kV. Data were recorded in the 5–60° 2θ range (step size 0.019732° and 0.5 s counting time for each step).

The thermal stability of the glass frits was analysed by differential thermal analysis (DTA) on both powder (< 63 μm) and bulk or monolithic (2 × 2 × 3 mm) glass samples. DTA runs were performed from room temperature to 1400 °C, at a heating rate of $50°C \cdot min^{-1}$ under flowing air in a Setaram Labsys Thermal Analyser. Samples of 40 mg were placed in platinum crucibles and calcined Al_2O_3 was used as the reference material. DTA curves were normalised with respect to the sample weight.

The occurrence of phase separation in the glass frits was studied by field emission scanning electron microscopy (FESEM) with a HITACHI S-4800P microscope using an acceleration voltage of 20 kV. Fresh fracture surfaces were etched for 10 s in a solution of 5% HF, ultrasonically washed with distilled water and ethylic alcohol, dried and coated with Au-Pd in a Balzers SCD 050 sputter.

Finally, the characterization of samples was completed by Fourier transform infrared (FTIR) spectroscopy in a Nicolet Nexus 670-870 equipment. FTIR spectra were recorded in the range of 400-4000 cm^{-1} by means of transmission measurements from sample diluted in KBr.

3. Results and discussion

The macroscopic appearance of the frits obtained in both electric and solar furnace are depicted in Figure 3. Appreciable differences are not observed.

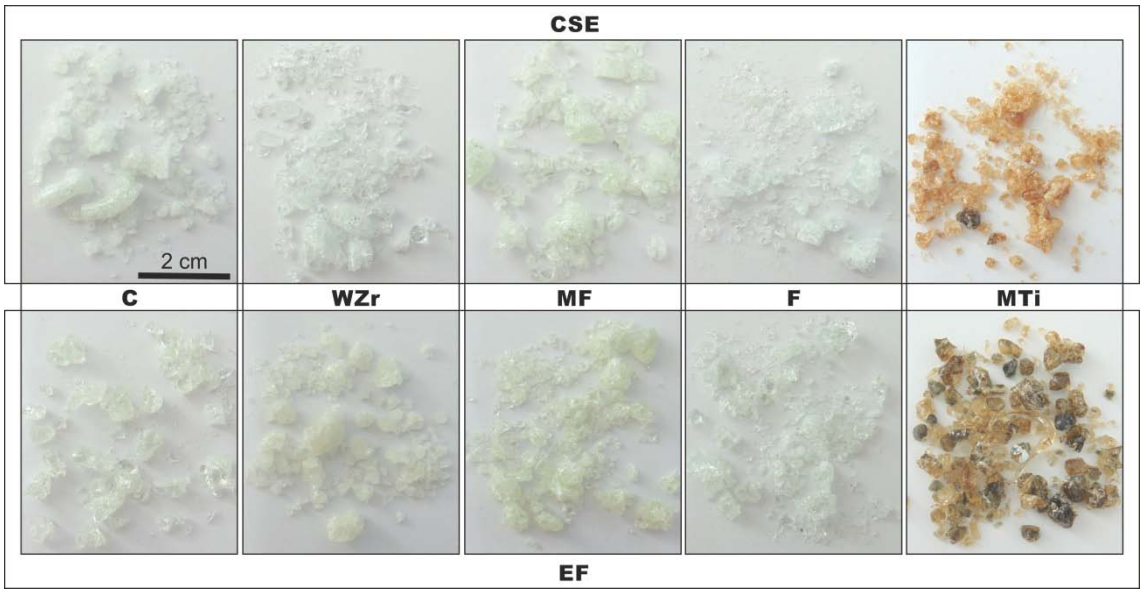

Fig. 3 Macroscopic appearance of frits obtained in electric furnace and by CSE

3.1. Chemical composition of glass frits

The chemical composition of the frits obtained in both experiments -CSE and electric furnace- determined by XRF and ICP-OES is shown in Table 2.

Table 2. Chemical composition (wt. %), of the frits prepared in both electric furnace (EF) and by CSE.

Frit	C		WZr		MF		F		MTi	
	EF	CSE	EF	CSE	EF	CSE	EF	CSE	EF	CSE
SiO_2	50.30	52.60	43.47	50.52	37.88	40.19	47.04	53.72	41.09	41.81
B_2O_3	9.75	11.80	8.74	10.60	5.84	7.12	11.80	13.4	14.60	15.10
Al_2O_3	11.50	5.83	22.50	5.71	11.0	3.98	15.00	2.24	7.76	4.02
Na_2O	3.60	3.97	--	--	4.10	4.70	9.07	11.1	2.13	2.65
K_2O	--	--	--	--	--	--	6.67	8.74	--	--
Li_2O	1.83	2.59	3.67	5.13	1.71	2.24	--	--	1.28	1.63
CaO	4.33	4.43	3.34	4.39	5.80	6.23	9.35	10.03	--	--
BaO	1.91	2.33	1.54	2.29	1.71	2.24	--	--	--	--

ZnO	5.27	5.38	6.40	8.10	3.00	3.16	--	--	1.69	1.69
PbO	10.49	10.05	--	--	28.18	29.52	--	--	24.35	25.59
ZrO_2	--	--	8.27	11.25	--	--	--	--	--	--
TiO_2	--	--	--	--	--	--	--	--	6.44	6.86

It can be seen that the melting process in a conventional electric furnace (EF) originates a high level of corrosion of the crucible wall by the melt, as denoted by the noticeable increasing of alumina content in the final frit composition. Thus, Al_2O_3 is detected even in the composition of F frit, in which alumina was not added to the raw materials batch. Figure 4 depicts the increasing in Al_2O_3 content in the final glass composition as result of the dissolution of the crucible components in the molten glass. As expected, in general the corrosion of crucible is higher as the viscosity of the melt is lower because as the Poiseuille's Law states, in Newtonian fluids the melt flowrate is linearly dependent to the inverse of the viscosity. Moreover, B_2O_3 losses by volatilization of boron are also detected (Fig. 4). It is noticeable that both Al_2O_3 dissolution and B_2O_3 volatilization take place in lower extend when the glass is molten by using concentrated solar energy. This result can be attributable to the shorter time required for accomplishing the whole melting by CSE. The use of high power density, as provided by the solar concentrator, allows reducing the process time in about 80% in contrast with the long time required to obtain the same material in a conventional electric furnace (Fig. 2). A lower time involves minor crucible corrosion since the rate of melt penetration is affected by time, in addition to other factors such as the open pore radius, slag viscosity, surface tension, etc. (Lee and Zhang, 2004). The variation of the rest of components in the composition of frits corresponds to the adjustment of the mass balance.

Therefore, these results indicate that the preparation of glass frits by the use of CSE leads to a very lower crucible corrosion. It is of great economic importance, since corrosion is one of the factors that contributes more to the decrease in the useful life of industrial refractory components.

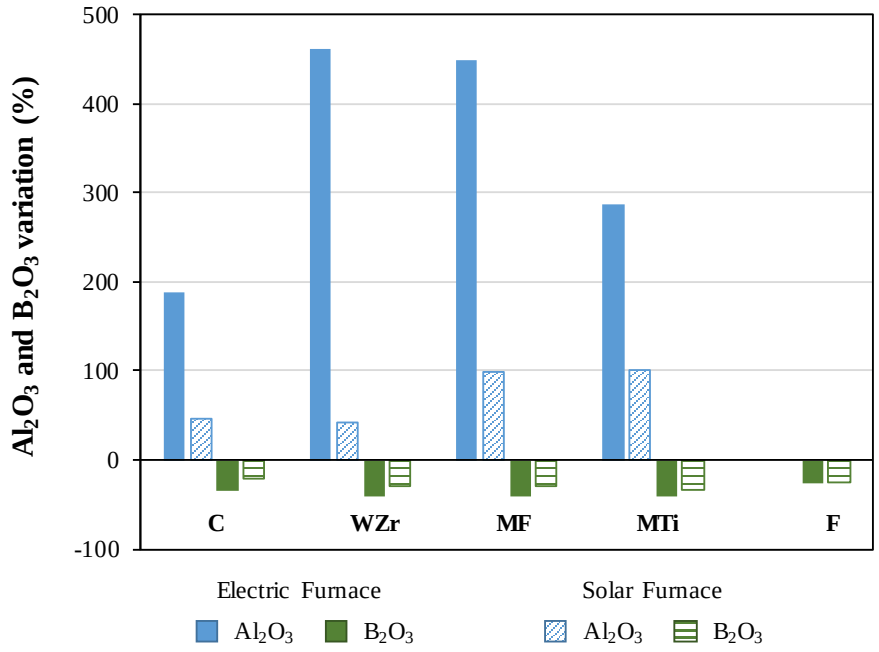

Fig. 4. Al_2O_3 dissolution and B_2O_3 volatilization during melting in EF and by CSE

3.2. Powder X-ray diffraction analysis

Figure 5 presents the XRD patterns corresponding to frits obtained by the two methods. It can be observed that the XRD profiles of all frits (except the corresponding to WZr frit prepared in EF) only show the characteristic amorphous halo of vitreous materials, in which any diffraction peaks due to crystalline phases are detected. However, the XRD profile of the frit with the higher melting temperature (WZr) shows small diffraction peaks that can be attributed to monoclinic phase of ZrO_2 (badeleyite), which indicates that this raw material was not completely incorporated into the melt during the melting process in the electric furnace and thus, it remains in the final glass frit.

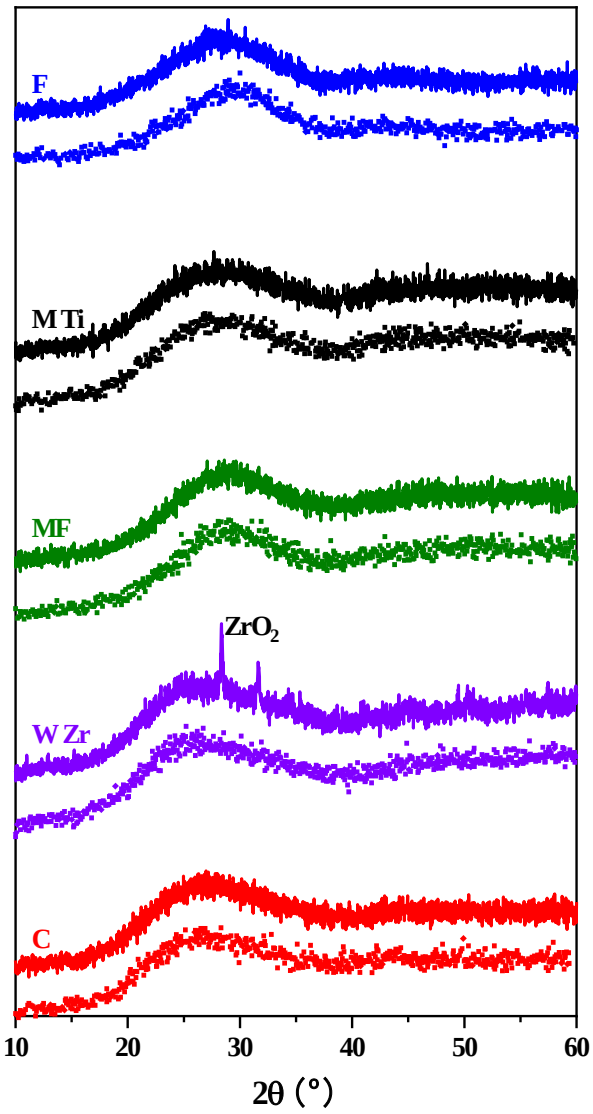

Fig. 5. XRD patterns of the glass frits obtained in solar furnace (dot line) and electric furnace (solid line).

Besides, it can be observed that the XRD profiles are very similar for each different type of frits. Glasses have no long-range order and are macroscopically isotropic in nature. However, the X-ray amorphous pattern is a finger print of the short-range order. It is worthy that in spite of the shorter time used in the solar melting process; the structures of the glass network of resulting glass frits are comparable.

3.3 Scanning electronic microscopy

For WZr frit, FESEM observations on a fresh fracture surface show that crystals are homogeneously dispersed within the parent WZr frit melted in conventional electric furnace. Figure 6 presents a detail of the observed microstructure, EDS analysis verify that non-reacted material is mainly badeleyite (98% ZrO_2) whereas the composition analysed in the parent glass (47.01 SiO_2, 24.05 Al_2O_3, 4.66 CaO, 1.29 Na_2O, 9.80 ZnO, 13.20 ZrO_2 wt. %) is close to that determined by XRF. This result presupposes an additional advantage to the use of concentrated solar energy for obtaining glass frits because this new process will allow melting and homogenisation of melts from batch compositions with high content of refractory oxide, which would be hardly melted in conventional furnaces.

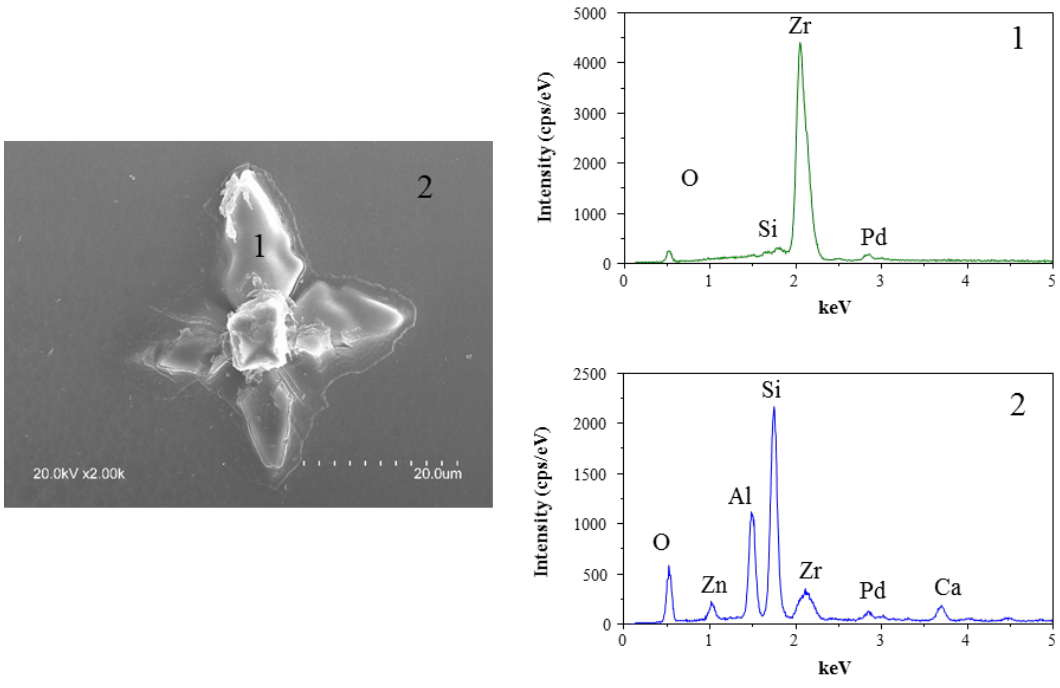

Fig. 6. FESEM observations on a fresh fracture surface of WZr frit melted in conventional electric furnace and EDS analyses recorded in both zirconia crystals and parent glass.

The microstructure observed with FESEM in the different frits studied in this work evidences glass-in-glass phase separation. As an example, Figure 7 shows FESEM observations on MF frits prepared in electric furnace and with CSE. Several cracks produced by the leaching stage used in sample preparation. Both melting processes bring about immiscible liquids in the glass during cooling. The result is a spinodal decomposition, which is characterised by the separation of non-spherical particles or drops with high connectivity. The FESEM images were analysed with ImageJ free software (https://imagej.nih.gov/ij/) in order to determine the effect of the melting process on phases separation. Results indicate that the microstructural parameters such as the density of drops and the average drop surface are not affected. Thus, the values obtained for frits prepared in electric furnace and by CSE are quite similar ($1.41x10^4$ drops/μm^2 and 70.73 nm^2 for electric furnace sample and $1.50x10^4$ drops/μm^2 and 66.66 nm^2 for sample obtained by CSE).

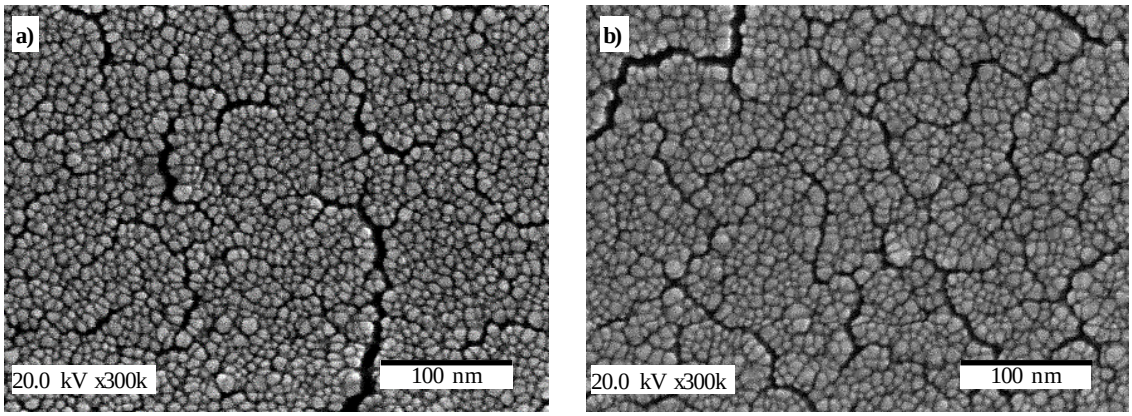

Fig. 7. FESEM observation showing glass-in-glass phase separation in MF frits prepared with a) concentrated solar energy and b) in electric furnace.

3.4. Thermal Analysis

The thermal behaviour of the glass frits was evaluated by DTA. Figure 8 shows the DTA curves of the glass frits produced by using CSE and in an electric furnace. In

general, the curves corresponding to each frit type shows a similar profile, which again denotes that the structure of the final frits prepared by CSE must be analogous to that of frits processed in an electric furnace. All the thermograms show the distinctive endothermic fall in the baseline corresponding to the glass transition temperature (Tg). In all cases, frits prepared by the use of concentrated solar energy show Tg values lower than those corresponding to frits produced in electric furnace. This result is likely due to differences observed in glass frits compositions.

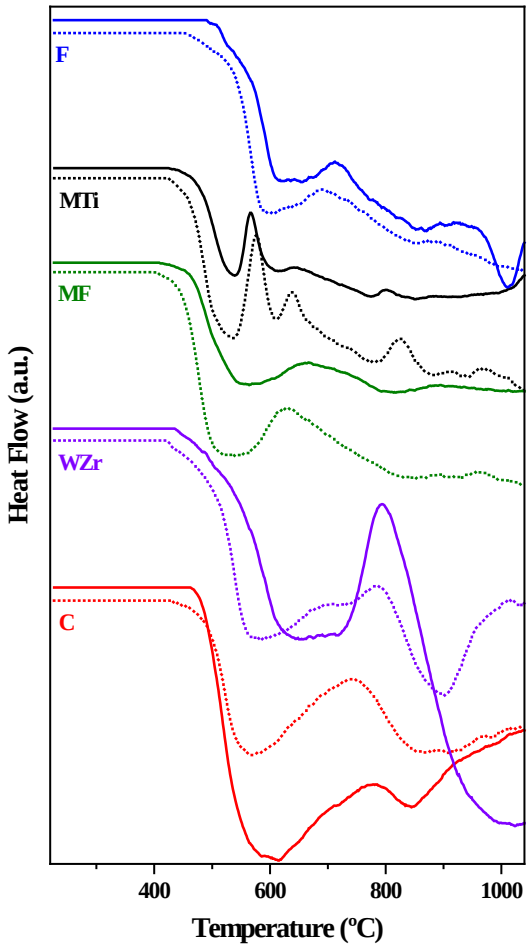

Fig. 8. DTA curves recorded from glass frits prepared with concentrated solar radiation (dot line) and in electric furnace (solid line).

As above mentioned (Table 2), the short thermal schedule used in solar experiments leads to a lower corrosion of the melt against the walls of the refractory crucibles, thus

incorporating low content of alumina to the final glass frit composition. Moreover, boron volatilization is also lower during the melting with direct solar radiation. As result, the final composition of the glass frits prepared in experiments performed with CSE showed higher content of fluxing oxides and they will lead to lower viscosity liquids and therefore, to lower Tg values. At higher temperatures, the DTA curves show different exothermic bands indicating that subsequent heat treatments of these glass frits could lead to the devitrification of crystalline phases.

MTi composition is the one showing a best defined devitrification process in the DTA curves of frits prepared by both CSE and in electric furnace. In this case, the effect of the melting process on the subsequent crystallization of the frit was evaluated by establishing the glass stability (GS), which symbolizes the resistance of a glass to crystallisation on heating; and the predominant devitrification mechanism for each frit. GS was evaluated by means of the working range ΔT_{TS} (Weinberg, 1994), whereas the predominant devitrification mechanism through the crystallisation temperature difference between fine and coarse frit samples, ΔT_p (Thakur and Thiagarajan, 1966), as follows:

$$\Delta T_{TS} = T_x - T_g \quad (1)$$

$$\Delta T_p = T_{p(fine)} - T_{p(coarse)} \quad (2)$$

where T_g, T_x and T_p are the glass transition temperature, onset and peak crystallisation temperatures, respectively.

Figure 9 presents the DTA curves of MTi frit recorded from samples with two different particle sizes, i.e., fine (< 63 μm powder) and coarse (small fragment) samples. The glass transition temperature (Tg) is an intrinsic property of the glass and hence, for a

given MTi frit, the Tg value is constant regardless of the particle size of the sample. Figure 8 indicates that in the process of devitrification of MTi frits coexist two crystallization mechanisms (surface and bulk) since DTA curves of glass samples with different particle sizes have well-defined exothermic peaks. Moreover, none mechanism seems to be predominant over the other since the area under the crystallization peak is similar in curves recorded from both fine and coarse samples. Table 3 report the values of the characteristic temperatures (T_g, T_x and T_p) derived from the DTA curves as well as the calculated values of ΔT_{TS} and ΔT_p. It is observed that in MTi frit, the use of concentrated energy radiation has a negligible effect on the onset of crystallization and only the position of the maximum of the crystallization peak is lightly affected. ΔT_{TS} is an indicative of the thermal stability of the glass so that the lower the value of ΔT_{TS}, the lower is the thermal stability of the glass and the easier it is to develop crystalline phases during heating (Donald et al., 2006). In this case, the values of ΔT_{TS} determined from MTi frit melted in an electric furnace is slightly lower, indicating that use of CSE leads to frits that are thermally more stable. Concerning the crystallization mechanisms, in glasses with $\Delta Tp > 0$ the devitrification process will start with the growth of crystals in the bulk of the glass particles, whereas the first crystal nuclei will develop on the surface of the glass grains when $\Delta Tp < 0$. The values of ΔTp determined from MTi glass frits prepared by both concentrated solar radiation and electric furnace indicates that as early mentioned these glasses devitrify by a process in which surface and bulk crystallisation overlap; however the surface mechanism is slightly predominant since although ΔTp is close to zero its value is negative.

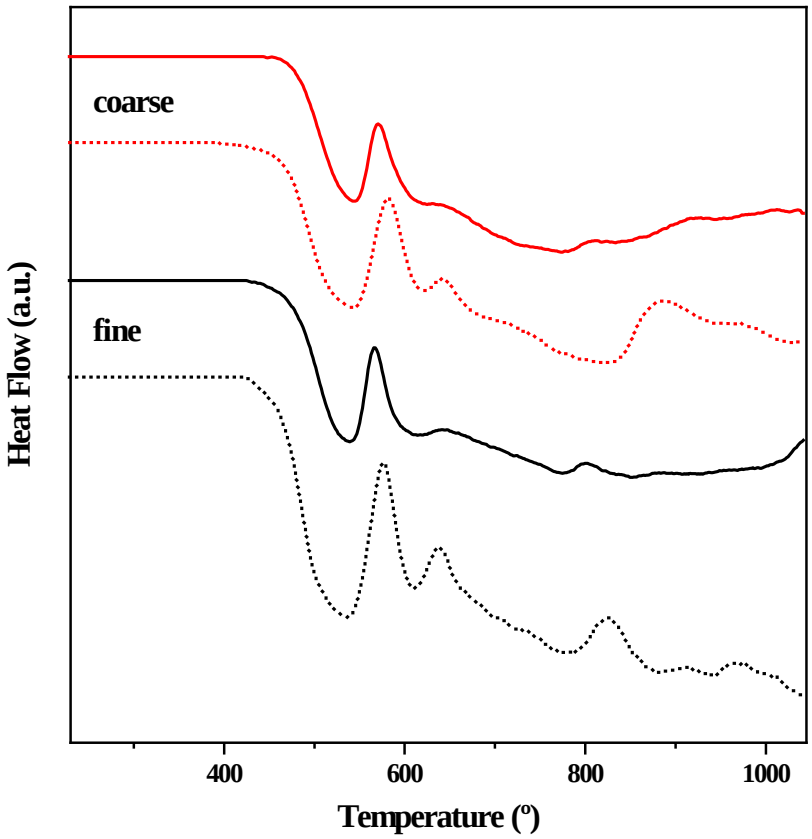

Fig.9. DTA curves of coarse and fine samples of MTi glass frits prepared with concentrated solar radiation (dot line) and in electric furnace (solid line)

Table 3. Characteristics temperatures derived from DTA curves for MTi frit and calculated ΔT_{TS} and ΔT_p values.

		Tg (ºC)	Tx (ºC)	Tp1 (ºC)	ΔT_{TS}	
CSE	Fine	488	549	576	61	ΔT_p (CSE) = -5 ΔT_p (EF) = -4
	Coarse	493	553	581	60	
EF	Fine	504	548	566	44	
	Coarse	505	551	570	46	

3.5. FTIR spectroscopy

Figure 10 shows FTIR transmission spectra of the studied glass frits. In general, the spectra of the different frits are similar and they show some specific bands within the range 400-1600 cm^{-1}. In silicate glasses, the structural unit in the glassy network is the silica tetrahedron [SiO_4] and thus their IR spectra depict vibrational bands due to bending, symmetric and antisymmetric stretching of the silicate units, which can be summarized as follows (Ibrahim et al., 2016): The bands centred at 450-470 cm^{-1} can be assigned to bending modes of Si-O-Si or O-Si-O (zone a). The weak peaks at 770-800 cm^{-1} can be attributed to Si-O-Si symmetric stretching vibrations of bridging oxygens between tetrahedral (zone b). The strong broad bands at 1000-1100 cm^{-1} can be related to Si-O-Si antisymmetric stretching of bridging oxygens within the tetrahedral (zone c). Vibrational bands corresponding to [AlO_4] are generally found in the same zones, and they are mostly undistinguishable because of the broadness of the bands. The studied frits include an important amount of boric oxide in their composition giving rise to the formation of structures in which [BO_3] and [SiO_4] coexists and in the FTIR are also detected the transmission spectra the vibrational bands due to borate units (Hivrekar et al., 2017), (Tamayo et al., 2009), such as a weak peak at 680-715 cm^{-1} can be assigned to bending vibrations of B-O-B (zone d) and a strong peak at 1410-1440 cm^{-1} can be attributed to vibration of B-O in boroxol rings (zone e). The small peak at 1620-1640 cm^{-1} is due to bending of O-H bond of molecular water (zone f). The pattern of sample MTi obtained in the electric furnace, a shoulder centred to 900 cm^{-1} can be attributable to Ti–O–Ti stretching vibration or even to Ti-O-Si stretching because of the presence of TiO_2 affects the silicate network structure. (Park et al., 2012), thus this sample exhibits the highest value for the Si-O-Si antisymmetric stretching and the lowest for the Si-O-Si

symmetric stretching. For sample WZr, the shoulder observed at 545 cm^{-1} could be tentatively assigned to Zr-O vibrations (Jayakumar et al., 2011).

Overall, for each frit category the spectrum corresponding to both melting processes shows a comparable shape. However, the IR curves recorded from frit samples prepared with CSE depict lower intensity band, being this difference more evident in the spectra belonging to WZr and MTi frits. This finding point out that the use of concentrated solar energy results in more amorphous frits when compared with those melted in conventional electric furnace. Indeed, XRD study of WZr frit (Fig. 5) brought to light the occurrence of a small amount of ZrO_2 in the frit prepared by conventional melting.

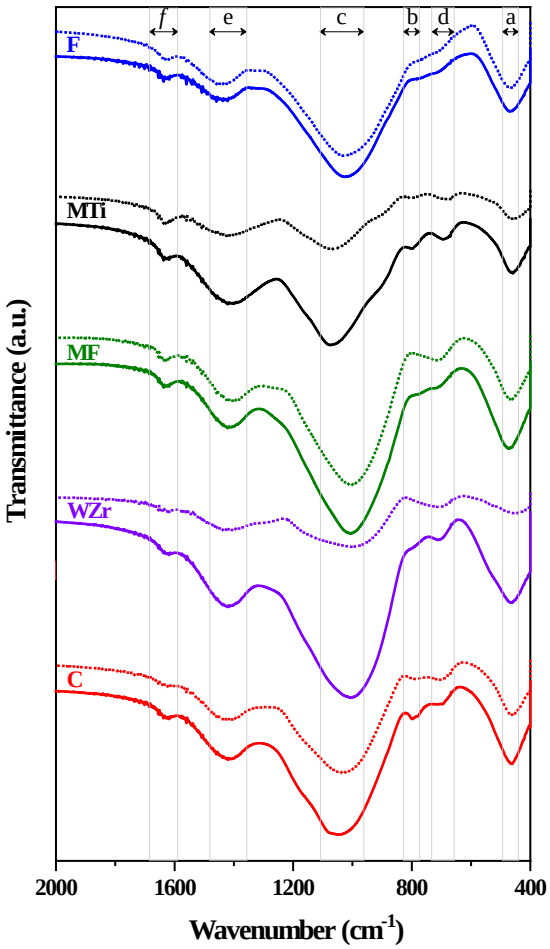

Fig.10. FTIR spectra of glass frits prepared with concentrated solar radiation (dot line) and in electric furnace (solid line).

3.6 Eco-efficiency

According to Scalet et al. (Scalet et al., 2013), the real energy consumption for modern industrial glass melting can vary from 3.5 to 40 GJ/t depending on furnace design and scale. The International Energy Agency (IEA) establishes the carbon dioxide emissions for electricity in Europe are 0.4537 kg CO2/kWh, these means that the corresponding emissions vary from 440 to 5040 kg CO2 per ton of glass frit which could be saved melting with CSE instead of electric furnace. Besides, taking into consideration the electricity cost in Spain is nowadays 0.13013€/kWh, the cost saving for the production of one ton of glass frit is about 723€. So the process described in this paper may be considered as eco-efficient. Nevertheless, a huge number of factor should be considered to estimate the real cost per ton of product, but future studies to design and evaluate the up-scaled plant costs are required.

4. Conclusions

The possibility of using direct concentrated solar energy for the melting of different glass compositions was studied for the first time. In view of the results, it can be highlighted that the use of CSE for manufacturing frits allows reducing the melting time in about 80%, which leads to both lower corrosion of crucible wall and lower volatilization of boron during the melting process. Glass frits melted by CSE show similar features when compared with those of frits melted from the same raw materials batch in an electric furnace. Accordingly, the structures of the glass network of resulting glass frits are comparable as denoted by DRX, DTA, FESEM and FTIR results, which indicate that in spite of the shorter time, the frits prepared by CSE present short-range

order, thermal behaviour and microstructure analogous to frits prepared in electric furnace.

Acknowledgements

Authors thank The European Solar Research Infrastructure for Concentrated Solar Power SFERA-II program" (EU.DG RTD's Project 312642), for providing the infrastructure used to develop the project EFFECF-P1602030188; and also CSIC for the project PIE 201550E012. The financial support through the project MAT2017-83025-R (Spanish Ministry of Economy, Industry and Competitiveness) is also recognized. The technical support of Mrs. P. Díaz and Mrs. E. Martín of the IETcc-CSIC and Mr. Florent Lecat of PROMES – CNRS is likewise appreciated.

References

Ahmad, S.Q.S., Hand, R.J., Wieckert, C., 2014. Use of concentrated radiation for solar powered glass melting experiments. Solar Energy 109, 174-182.

Costa Oliveira, F.A., Shohoji, N., Fernandes, J.C., Rosa, L.G., 2005. Solar sintering of cordierite-based ceramics at low temperatures. Solar Energy 78(3), 351-361.

de Damborenea, J., Vázquez, A.J., Fernández, B., 1994. Laser-clad 316 stainless steel with Ni □ Cr powder mixtures. Materials & Design 15(1), 41-44.

Donald, I.W., Metcalfe, B.L., Fong, S.K., Gerrard, L.A., 2006. The influence of Fe2O3 and B2O3 additions on the thermal properties, crystallization kinetics and durability of a sodium aluminum phosphate glass. Journal of Non-Crystalline Solids 352(28), 2993-3001.

Fluegel, A., 2007. Glass viscosity calculation based on a global statistical modelling approach. Glass Technology - European Journal of Glass Science and Technology Part A 48(1), 13-30.

Funken, K.-H., Roeb, M., Schwarzboezl, P., Warnecke, H., 2001. Aluminum Remelting using Directly Solar-Heated Rotary Kilns. Journal of Solar Energy Engineering 123(2), 117-124.

García, I., Gracia-Escosa, E., Bayod, M., Conde, A., Arenas, M.A., Damborenea, J., Romero, A., Rodríguez, G., 2016. Sustainable production of titanium foams for biomedical applications by Concentrated Solar Energy sintering. Materials Letters 185, 420-423.

Hivrekar, M.M., Sable, D.B., Solunke, M.B., Jadhav, K.M., 2017. Network structure analysis of modifier CdO doped sodium borate glass using FTIR and Raman spectroscopy. Journal of Non-Crystalline Solids 474, 58-65.

Ibrahim, M.M., Fanny, M.A., Hassaan, M.Y., ElBatal, H.A., 2016. Optical, FTIR and DC Conductivity of Soda Lime Silicate Glass Containing Cement Dust and Transition Metal Ions. Silicon 8(3), 443-453.

Jayakumar, S., Ananthapadmanabhan, P.V., Perumal, K., Thiyagarajan, T.K., Mishra, S.C., Su, L.T., Tok, A.I.Y., Guo, J., 2011. Characterization of nano-crystalline ZrO2 synthesized via reactive plasma processing. Materials Science and Engineering: B 176(12), 894-899.

Lee, W.E., Zhang, S., 2004. Direct and indirect slag corrosion of oxide and oxide-c refractories, VII International Conference on Molten slags, fluxes & salts. The South African Institute of Mining and Metallurgy Johannesburg, Republic of South Africa, pp. 309-319.

López-Delgado, A., López-Andrés, S., Padilla, I., Álvarez, M., Galindo, R., Vázquez, A.J., 2014. Dehydration of Gypsum Rock by Solar Energy: Preliminary Study. Geomaterials 4, 82-91.

Meier, A., Gremaud, N., Steinfeld, A., 2005. Economic evaluation of the industrial solar production of lime. Energy Conversion and Management 46(6), 905-926.

Morris, D.G., López-Delgado, A., Padilla, I., Muñoz-Morris, M.A., 2015. Selection of high temperature materials for concentrated solar power systems: Property maps and experiments. Solar Energy 112, 246-258.

Otmakhov, V.I., 2015. Firing of Glass Enamel by Concentrated Solar Radiation. Glass and Ceramics 72(7), 266-268.

Padilla, I., López-Delgado, A., López-Andrés, S., Álvarez, M., Galindo, R., Vázquez-Vaamonde, A.J., 2014. The Application of Thermal Solar Energy to High Temperature Processes: Case Study of the Synthesis of Alumina from Boehmite. The Scientific World Journal 2014, 7.

Park, H., Park, J.-Y., Kim, G.H., Sohn, I., 2012. Effect of TiO2 on the Viscosity and Slag Structure in Blast Furnace Type Slags. steel research international 83(2), 150-156.

Román, R., Cañadas, I., Rodríguez, J., Hernández, M.T., González, M., 2008. Solar sintering of alumina ceramics: Microstructural development. Solar Energy 82(10), 893-902.

Romero, A., García, I., Arenas, M.A., López, V., Vázquez, A., 2013. High melting point metals welding by concentrated solar energy. Solar Energy 95, 131-143.

Scalet, B.M., Garcia Muñoz, M., Sissa, A.Q., Roudier, S., Delgado Sancho, L., 2013. Best available techniques (BAT) reference document for the manufacture of glass. . Luxembourg: Publicarions Office of the European, 2013, pp. 1-485.

Sierra, C., Vázquez, A.J., 2005. NiAl coatings on carbon steel by self-propagating high-temperature synthesis assisted with concentrated solar energy: mass influence on adherence and porosity. Solar Energy Materials and Solar Cells 86(1), 33-42.

Tamayo, A., Pérez-Villar, S., Rubio, F., Rodríguez, M.A., Rubio, J., Oteo, J.L., 2009. Caracterización estructural de vidrios del sistema SiO_2- B_2O_3-Na_2O- mediante espectroscopías IR y Raman. Boletin de la Sociedad Española de Cerámica y Vidrio 48(5), 237-243.

Thakur, R.L., Thiagarajan, S., 1966. Studies in catalyzed crystallization of glasses: a DTA method. Central Glass and Ceramic Research Bulletin 13, 33-45.

Trier, W., 1987. Glass furnaces: design, construction and operation. Society of Glass Technology, Sheffield.

Tzouganatos, N., Matter, R., Wieckert, C., Antrekowitsch, J., Gamroth, M., Steinfeld, A., 2013. Thermal Recycling of Waelz Oxide Using Concentrated Solar Energy. JOM 65(12), 1733-1743.

Vázquez, A.J., Rodriguez, G.P., de Damborenea, J., 1991. Surface treatment of steels by solar energy. Solar Energy Materials 24(1), 751-759.

Weinberg, M.C., 1994. An Assessment of Glass Stability-Criteria. Physics and Chemistry of Glasses. Society of Glass Technology 35(3), 119 - 123.